



Semnan University



Mixed convection study in a ventilated square cavity using nanofluids

Paulo Mohallem Guimarães^{a*}, Márcio Dimas Ramos^a, Genésio José Menon^b

^aFederal University of Itajubá at Itabira, Irmã Ivone Drumon St., 200, Industrial District II, Itabira-MG, 35903087, Brazil.

^bFederal University of Itajubá at Itajubá, BPS Ave., 1303, Pinheirinho District, Itabira-MG, 37500903, Brazil.

PAPER INFO

Paper history:

Received: 2018-04-28

Received: 2018-11-08

Accepted: 2018-12-03

Keywords:

Nanofluids,
Mixed convection,
Finite element method.

ABSTRACT

This work indicates a numerical study on the laminar heat transfer mixed convection in a square cavity with two openings (an inlet and an outlet) on vertical walls through which nanofluid flows. Two flow directions are examined: i) ascending flow which enters the bottom opening and exits the upper opening; ii) descending flow which enters the upper opening and exits the bottom opening. The ascending flow contributes to buoyancy forces while for the descending flow, the opposite takes place. The intention is to cool a heat source placed at the center of the geometry. The nanofluid has Copper nanoparticles and water as its base-fluid. The velocity and temperature of the entrance flow are known. Some results are experimentally and numerically validated. A mesh independency study is carried out. Some parameters are ranged as follows: i) the Reynolds number from 50 to 500, the nanofluid volume fraction from 0 to 1%, the Grashof number from 10^3 to 10^5 . It is noteworthy to mention that in some cases, the fluid is stuck inside the cavity which weakens the heat transfer. The nanoparticles increase the heat transfer of 4% for the ascending primary flow inside the cavity.

DOI: 10.22075/jhmtr.2018.14640.1208

© 2019 Published by Semnan University Press. All rights reserved.

1. Introduction

The study of nanofluid behavior in engineering problems has had an enormous advance in recent years as a result of computational increasing power, not only in what deals with more powerful machines, but in techniques and in commercial software for numerical simulation as well. Moreover, nanofluid application in order to enhance heat transfer has been successful and has been given special attention by the scientists in some areas such as: i) heat exchangers; ii) medicine transport inside human body, electronic components, solar collectors and so on. A feature of the present study is to apply nanofluid as the refrigerant fluid in order to cool a heat source that can be extended to heat exchangers.

Moumni et al. [1] accomplished a numerical analyses in a partially heated ventilated square cavity undergoing a laminar regime and mixed convection heat transfer. The

nanofluid has water as its base-fluid and Cu nanoparticles. Some parameters were ranged as follows: Richardson number from 0.1 to 10, Reynolds number from 10 to 500, and solid volume fraction from 0 to 0.1. They concluded that by increasing concentration, Reynolds number and Richardson number, the rate of heat transfer enhanced. They also found out that the highest heat transfer occurred on the right part surface of the heat source, no matter the parameter analysed in their work.

Hinojosa et al. [2] performed an analyses on the heat transfer of turbulent mixed convection of air flow in a vented enclosure. Two vertical walls were heated in different ways: one at a constant heat flux and the other at a certain constant temperature profile. All remaining walls were thermally insulated. The experimental temperature behaviors were achieved for various heat fluxes and entrance velocity profiles. They applied different

* Corresponding Author: P. M. Guimarães, Federal University of Itajubá at Itabira, Irmã Ivone Drumon St., 200, Industrial District II, Itabira-MG, 35903087, Brazil.

Email: pauloguimaraes@unifei.edu.br

turbulence models. When comparing the turbulence approaches with experimental results, the standard $k-\epsilon$ turbulence model displayed a better result closeness in temperature, with the highest percentage differences ranging from 2.0% to 3.0%. The convective heat transfer coefficient ranged from 2.2 to 3.4W/m²K. It increased when increasing the Rayleigh and the Reynolds numbers as well.

A study was conducted on the heat and fluid flow features when decreasing temperatures in a set of discrete protruding heated sources in channels by forcing a laminar flow of air jet (Arquis et al. [3]). They obtained numerical results for various values of Reynolds number, heights of channel, distance between hot bodies, body height, and thermal conductivity of heated modules. Some parameters were varied and exhibited the importance of some results which are significant to the control of electronic set temperature. Overall, the effective temperature decrease of bodies enhanced while Reynolds number increased and the channel height decreased. Recirculation cells which appeared on the top surface of the downstream bodies helped the Nusselt number decrease. The region where the average Nusselt number reached its maximum on the body surface was beneath the place where the air was impinged. Due to the thermal wake, the temperature went up for downstream bodies, and almost reached a constant value after the third body.

Madhusudhana & Narasimham [4] conducted a numerical work on conjugate mixed convection in heat generating ribs placed on substrates composing vertical arrays in a set of channels that were equally placed. The boundary conditions were periodic in the cross-cut direction with equal arrangement and heat generating protruding bodies on each plate. The control volume approach was performed in order to discretize the governing equations by the concept of staggered mesh and the pressure term was corrected by a coupling technique of pressure and velocity. The rigid locations were regarded as fluid zones with a very large viscosity. The thermal energy interaction of solid and fluid zones was considered when applying the harmonic thermal conductivity technique. Heat generation was varied when ranging the Grashof number from 10^4 to 10^7 . The air velocity was considered by ranging the Reynolds number from 0 to 1500. The induced mass flow rate changed of the order of 0.44 power of Grashof number in pure natural convection. The heat conducted to air through the substrate was 41 to 47% of the total heat removed from the bodies.

Shahi et al. [5] carried out a study on mixed convection by applying nanoparticles of Copper and water as the basis-fluid of the nanofluid in a ventilated square cavity. Buoyancy forces appeared a constant flux heat source placed on the bottom wall. The approximated solutions were reached by using the finite volume method and SIMPLE algorithm with collocation method. The analyses was performed for the following: i) Reynolds number from 50 to 1000, ii) Richardson number from 0 to 10, iii) the nanoparticle concentrations from 0 to 0.05. Patel and

Brinkman models were applied to consider the nanofluid thermal conductivity and effective viscosity, respectively. They also revealed the effects of nanofluid volume fraction on the fluid flow and heat transfer features. The increase in solid concentration provided a Nusselt number increase on the heated module surface which is also associated to a mean temperature decrease.

Nassan et al. [6] presented a research on the heat transfer in a square transverse cupric channel. The flow regime was laminar and the duct underwent a uniform heat flux. The heat transfer was compared by applying two nanofluids: Al₂O₃/water and CuO/water nanofluids. Some situations presented the need for channels which are not circular. Consequently, a testing facility was built as a result to pressure drop drawbacks. Experimental studies were conducted with distinct concentrations in the nanofluid having pure water as its base fluid. The resulting effects indicates that a relevant heat transfer improvement was achieved by all nanofluids when comparing to the case with distilled water only. Nonetheless, monoxide Copper nanofluid showed heat transfer enhancement compared with Alumina nanofluid.

Rostamani et al. [7] conducted a numerical study on turbulent nanofluid flow and various volume concentrations of nanoparticles. The flow was inside a two-dimensional channel undergoing steady heat flux boundary condition. The nanofluids were mixtures of copper oxide (CuO), or alumina (Al₂O₃), or oxide titanium (TiO₂) nanoparticles, and water as their base fluid. All thermophysical properties of nanofluids were dependent of temperature. The nanofluid viscosity was experimentally achieved. Additionally, they performed a comparison analyses of the Nusselt numbers that showed good agreement with Gnielinski's correlation. The study pointed out that with the volume concentration increase, the wall shear stress and heat transfer rates were augmented. By keeping constant volume concentration and constant Reynolds number, the effect of CuO nanoparticles appeared to increase the Nusselt number. Al₂O₃ and TiO₂ nanoparticles did not enhance the heat transfer in a same way, though.

Lotfi et al. [8] performed a forced convection study in horizontally-placed pipes in which nanofluid flows. The nanofluid consists of water and nanoparticles of Al₂O₃. They also conducted validations with benchmark problems applying well stated correlations found in literature. An Eulerian model was utilized in a two-phase technique. The comparison using experimental values showed that the mixture model was more accurate. The single-phase and the two-phase Eulerian models underestimated the Nusselt number.

Jung et al. [9] investigated the behavior of heat transfer and friction parameters of nanofluid flowing in rectangle-shaped microchannels. They built a system comprising a single microchannel on one wall, a pair of heated-modules and a set of polysilicon temperature meters spread on the opposite wall. They applied aluminum nanofluid dioxide (Al₂O₃) with a 170 nm-diameter. Different volume

concentrations were applied. The convection heat transfer of the Al₂O₃ nanofluid risen up to 32% in relation to the pure water at a volume fraction of 1.8 volume percent without significant waste. The higher the Reynolds number is, the higher the Nusselt number in the laminar regime.

Arefmanesh and Mahmood [10] examined laminar mixed convection regime in a square-shaped cavity having the non-accuracy in the effective absolute viscosity of nanofluid with Al₂O₃ and water as its basis-fluid. The two walls and the top wall had their temperature diminished in order to heat the cavity. The horizontal bottom lid-driven wall of the cavity was kept at a uniform temperature. The problem equations were given in terms of velocity, pressure and temperature. They were numerically solved by applying the finite volume technique. Two different approaches for the nanofluid absolute viscosity were carried out. They studied the behaviour of the Richardson number and the nanoparticle concentration on the velocity and temperature profiles in the cavity. For the two viscosity models utilized, there were significant differences in Nusselt increase in the cavity. Moreover, overall, the mean Nusselt number on the heated wall rose as the nanoparticle concentration increased for those two models of viscosity.

Behzardi et al. [11] suggested an analyses of numerical mixed convection heat transfer in order to examine the effect of a porous matrix in a vented square enclosure. The top and bottom walls of the enclosure were kept at constant temperature and at a constant heat flux, respectively. The right and left walls were adiabatic. The inlet and outlet flow surfaces were positioned on left vertical wall and right vertical wall, respectively. They observed the behavior of the fluid flow and heat transfer rate by changing the Richardson number and the Darcy number. It was noted that the increasing Darcy number and porous particles diameter made heat transfer decrease.

2. Mathematical formulation

The aim of this research is to present numerical analyses on the mixed convection inside a vented square cavity in the laminar regime. Inside this cavity, there is a square heat source. In this article, the flow can go upwards (it comes in through the lower part and comes out through the upper part of the cavity vertical walls) or downwards (just the opposite for upwards flow). Every wall, except those of the heat source, are isolated and are under no-slip condition. The heated inner square has constant and uniform heat flux. The nanofluid is composed of water and copper nanoparticles. At the inlet, there is a constant velocity and low temperature profiles, while at the outlet, symmetry conditions are applied. The nanoparticle volume-fraction is 1% by reason of the thermophysical property correlations used. Figure 1 depicts the geometry and boundary conditions of the problem. The dimensionless velocities on X and Y directions are U and V, respectively, the enclosure width (W), the enclosure height (H), the dimensionless temperature θ , and the

nanofluid properties are the density (ρ_{nf}), the dynamic viscosity (μ_{nf}) and the thermal conductivity (k_{nf}).

The dimensional equations of conservation of mass, momentum and energy are, respectively:

$$\frac{\partial u}{\partial x} + \frac{\partial v}{\partial y} = 0 \tag{1}$$

$$u \frac{\partial u}{\partial x} + v \frac{\partial u}{\partial y} = \frac{1}{\rho_{nf}} \left[-\frac{\partial p}{\partial x} + \mu_{nf} \left(\frac{\partial^2 u}{\partial x^2} + \frac{\partial^2 u}{\partial y^2} \right) \right] \tag{2}$$

$$u \frac{\partial v}{\partial x} + v \frac{\partial v}{\partial y} = \frac{1}{\rho_{nf}} \left[-\frac{\partial p}{\partial y} + \mu_{nf} \left(\frac{\partial^2 v}{\partial x^2} + \frac{\partial^2 v}{\partial y^2} \right) \right] + [(\rho\beta)_{nf} (T - T_c)] g \tag{3}$$

$$u \frac{\partial T}{\partial x} + v \frac{\partial T}{\partial y} = \alpha_{nf} \left(\frac{\partial^2 T}{\partial x^2} + \frac{\partial^2 T}{\partial y^2} \right) \tag{4}$$

where u and v are the velocities, p is the pressure, T is the temperature, ρ_{nf} is the nanofluid density, μ_{nf} is the nanofluid absolute viscosity, α_{nf} is the nanofluid thermal diffusivity, C_p is the nanofluid heat capacity and β_{nf} is the nanofluid thermal expansion coefficient.

The effective nanofluid density and the nanofluid thermal diffusivity are:

$$\rho_{nf} = (1 - \phi) \rho_f + \phi \rho_p \tag{5}$$

$$\alpha_{nf} = k_{nf} / (\rho C_p)_{nf} \tag{6}$$

where ϕ is the concentration of solid nanoparticles.

The subscripts f and p refer to fluid and particles, respectively. Copper (Cu) nanoparticle is considered in this study. The base fluid is water with Prandtl number (Pr) equal to 6.2.

Table 1 indicates the thermophysical properties of water and Copper nanoparticles.

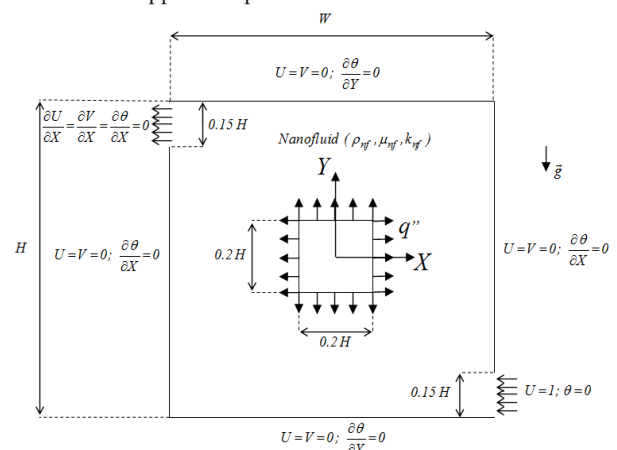


Figure 1. Geometry and boundary conditions

Table 1. Thermophysical properties

Thermophysical properties	Fluid Phase (water)	Cu
Cp (J/kgK)	4179	385
ρ (kg/m ³)	997.1	8933
K (W/mK)	0.613	400
$\beta \times 10^{-5}$ (1/K)	21	1.67

Other thermophysical parameters of the nanofluid are: the heat capacitance $(\rho C_p)_{nf}$, the thermal expansion $(\rho\beta)_{nf}$, and the dynamic viscosity $(\mu)_{nf}$ (Brinkman model [12]). They are given by:

$$(\rho C_p)_{nf} = (1-\phi)(\rho C_p)_f + \phi(\rho C_p)_p \quad (7)$$

$$(\rho\beta)_{nf} = (1-\phi)(\rho\beta)_f + \phi(\rho\beta)_p \quad (8)$$

$$\mu_{nf} = \frac{\mu_f}{(1-\phi)^{2.5}} \quad (9)$$

Equation (10) gives the thermal conductivity k_{nf} , for spherical particles and it is based on Maxwell –Garnett's model [13], given by:

$$k_{nf} = k_f \left[\frac{(k_p + 2k_f) - 2\phi(k_f - k_p)}{(k_p + 2k_f) + \phi(k_f - k_p)} \right] \quad (10)$$

where k_p is the thermal conductivity of nanoparticle (Copper), and k_f is the thermal conductivity of the base fluid (water).

The Maxwell-Garnett's model has been used by some other researchers: Aminossadati and Ghasemi [14], Ho et al. [15] and Oztop and Abu-Nada [16].

With the intention to rewrite the equations in terms of dimensionless form, the following dimensionless parameters are considered:

$$\begin{aligned} X = \frac{x}{H}; Y = \frac{y}{H}; U = \frac{u}{u_0}; V = \frac{v}{u_0}; P = \frac{p}{\rho_{nf} u_0}; \theta = \frac{(T - T_c)}{(\Delta T)}; \\ Gr = \frac{g\beta_f H^3 \Delta T}{\nu_f^2}; \Delta T = \frac{q'' H}{k_f}; Pr = \frac{\nu_f}{\alpha_f}; Ri = \frac{Gr}{Re^2}; Re = \frac{u_0 H}{\mu_f} \end{aligned} \quad (11)$$

where U and V are the dimensionless velocities, P is the dimensionless pressure, θ is the dimensionless temperature, Gr is the Grashof number, Pr is the Prandtl number, Ri is the Richardson number, ν_f is the base-fluid kinematics viscosity, α_f is the base-fluid thermal diffusivity, and Re is the Reynolds number.

Substituting Eq. (11) into Eqs. (2), (3) and (4), the final form of the conservation equations is:

$$\frac{\partial U}{\partial X} + \frac{\partial V}{\partial Y} = 0 \quad (12)$$

$$U \frac{\partial U}{\partial X} + V \frac{\partial U}{\partial Y} = -\frac{\partial P}{\partial X} + \frac{1}{Re} \frac{\mu_{eff}}{\nu_f \rho_{nf}} \left(\frac{\partial^2 U}{\partial X^2} + \frac{\partial^2 U}{\partial Y^2} \right) \quad (13)$$

$$U \frac{\partial V}{\partial X} + V \frac{\partial V}{\partial Y} = -\frac{\partial P}{\partial Y} + \frac{1}{Re} \frac{\mu_{eff}}{\nu_f \rho_{nf}} \left(\frac{\partial^2 V}{\partial X^2} + \frac{\partial^2 V}{\partial Y^2} \right) + \frac{(\rho\beta)_{nf}}{\rho_{nf} \beta_f} Ri \theta \quad (14)$$

$$U \frac{\partial \theta}{\partial X} + V \frac{\partial \theta}{\partial Y} = -\frac{\alpha_{nf}}{\alpha_f} \frac{1}{Pr Re} \left(\frac{\partial^2 \theta}{\partial X^2} + \frac{\partial^2 \theta}{\partial Y^2} \right) \quad (15)$$

The local Nusselt number on a certain surface, which is directly dependent on the convection heat transfer coefficient h , is written as the following:

$$Nu_{hs}^* = \frac{hL}{k_f} \quad (16)$$

where:

$$h = \frac{q''}{T_s - T_c} \quad (17)$$

Substituting (11) and (17) into (16), then the local Nusselt number is:

$$Nu_{hs}^*(X, Y) = \frac{I}{\theta(X, Y)} \Big|_{hs} \quad (18)$$

where the subscript hs is the heater surface and S is the surface length where Nu_{hs}^* is integrated on. The average Nusselt number (Nu_{hs}) is given by:

$$Nu_{hs}(X, Y) = \frac{I}{S} \int_{hs} Nu_{hs}^* \quad (19)$$

3. Numerical procedure and validation

The approximated solution for Equations (12) to (15) is obtained by applying the finite element method (FEM). The Petrov-Galerkin technique is applied on convection terms. The pressure expressions are manipulated using penalty formulation with the penalty value equal to 10^9 . The authors utilized a numerical code applying the Fortran language. The first validation is about a benchmark problem involving natural convection in a square. This enclosure is differentially heated. The vertical wall dimensionless temperature profiles are uniform and equal to 0 and 1 on the cold and hot walls, respectively. The analyses is conducted by comparing the average Nusselt number along the heated wall, the highest velocities in the X and Y directions and their corresponding positions at Y and X axes, for Ra equal to 10^3 and 10^6 (Table 2). The working fluid is air with Pr equal to 0.7. Very good comparison closeness is obtained.

The second comparison is presented in Fig. 2. It illustrates the temperature and velocity behavior in the y-mid-section direction ($Y=0.5$). The geometry and boundary conditions are the same as the ones used in the first comparison. Ra is 1.89 and Pr is 0.71. Also, for such a case, some experimental results from Krane and Jessee [17] and numerical ones from Khanafer et al. [18] are given for comparison. An excellent agreement is achieved for both numerical and experimental studies.

The third validation is the same standard case applied previously in this work. Although the geometry is the same, the dimensionless temperatures on the isothermal vertical walls are different, that is, -1 and 1. In addition, they considered in their work air with Prandtl number Pr equal to 0.7, and Rayleigh numbers ranging from 10^3 to 10^5 . The temperature and v-velocity profiles are selected at $Y = 0.5$. The figures were contrasted with the ones presented in Khanafer et al. [18] and Fidap [19]. The pictures were exactly superposed and they had satisfactorily agreed. Table 3 presents the fourth validation, which is related to nanofluid behavior. Aminossadati and Ghasemi [14] presented this problem. The problem is about a square cavity with a heat source with length B which is located on the center of the bottom wall. All walls are at temperature equal to zero. The bottom wall is isolated, though. Water is utilized as its base fluid with $Pr = 6.2$. The nanoparticles used are Copper, Alumina and Titanium Oxide.

Table 2. Comparison-Square differentially heated cavity with wall temperatures 0 and 1.

	Present work	[18]	[20]	[21]	[22]
Nu	1.121	1.118	1.114	1.118	1.105
U_{max} (at y/H)	0.138 (0.812)	0.137 (0.812)	0.153 (0.806)	0.136 (0.813)	0.132 (0.833)
V_{max} (at x/H)	0.140 (0.178)	0.139 (0.173)	0.155 (0.181)	0.138 (0.178)	0.131 (0.200)
Nu	8.836	8.826	8.806	8.799	9.012
U_{max} (at y/H)	0.076 (0.850)	0.077 (0.854)	0.077 (0.859)	0.079 (0.850)	0.084 (0.856)
V_{max} (at x/H)	0.262 (0.038)	0.262 (0.039)	0.262 (0.039)	0.262 (0.038)	0.259 (0.033)

Table 3. Comparison for the case with a heater on the bottom of a square cavity with $\phi = 0.1$, $B = 0.4$ and $Pr = 6.2$.

	Num		Tmax	
	Present	[14]	Present	[14]
Ra=10 ³				
Cu	5.4681 (0.30%)	5.451	0.205 (0.00%)	0.205
Al ₂ O ₃	5.4075 (0.30%)	5.391	0.207 (0.00%)	0.207
TiO ₂	5.2058 (0.32%)	5.189	0.215 (0.00%)	0.215
Ra=10 ⁶				
Cu	13.5222 (2.53%)	13.864	0.109 (1.84%)	0.107
Al ₂ O ₃	13.4093 (1.89%)	13.663	0.110 (1.82%)	0.108
TiO ₂	13.1595 (1.95%)	13.416	0.113 (1.77%)	0.111

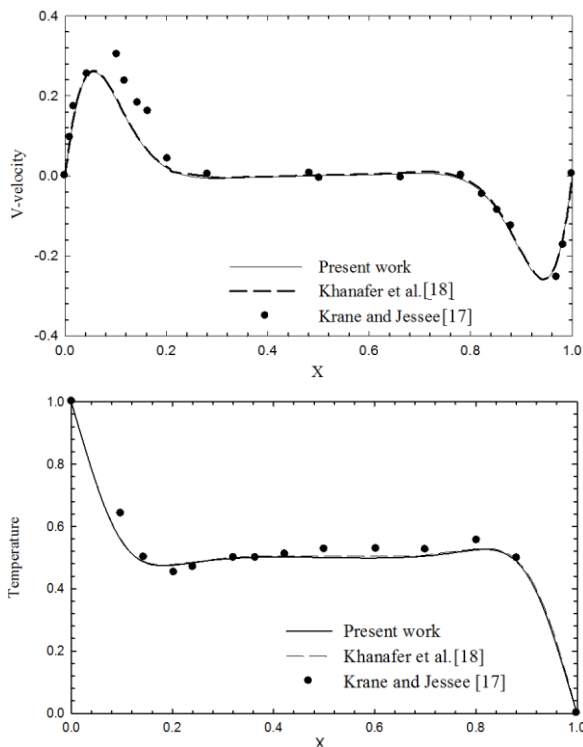


Figure 2. Comparison of velocity and temperature behavior in y-direction at $Y = 0.5$ for $Ra = 1.89$, $Pr = 0.71$.

One can observe results for average Nusselt number and maximum temperature on the heat source for Ra equal 10^3 and 10^6 . This comparison presents excellent agreement.

For the present work, two grids were studied applying non-structured 4-noded quadrilateral elements. One grid with 34774 elements and the other with 51388 elements (Fig. 3). A deviation of less than 1% was achieved. As a result of the variation of the element number and deviation, the grid with 51388 elements was applied. The reason for having such grid is the computing time needed to compute cases for two limits in terms of Grashof number and concentration, that is, $Gr = 10^3$ and $Gr = 10^5$, and $\phi = 0$ (pure water) and $\phi = 0.01$.

A special attention is dispensed to the elements near the wall where the average Nusselt numbers on the heat source and cold walls are going to be evaluated. The reason for that is that higher temperature gradients are predicted in those zones. The grid performance technique undergoes the minimum element angle criterion, that is, elements are arranged in order that element inner angles are arranged as close as 90° .

The hardware configuration used to run all cases has 6Gb of RAM and Intel®Core™ 2 Duo CPU P7350 2Ghz.

The convergence criterion to stop the program is:

$$Res = \frac{abs(Var(\tau_i) - Var(\tau_{i-1}))}{\Delta\tau} \leq 10^5 \tag{20}$$

$$\Delta\tau = \tau_i - \tau_{i-1} = 0.0001 \tag{21}$$

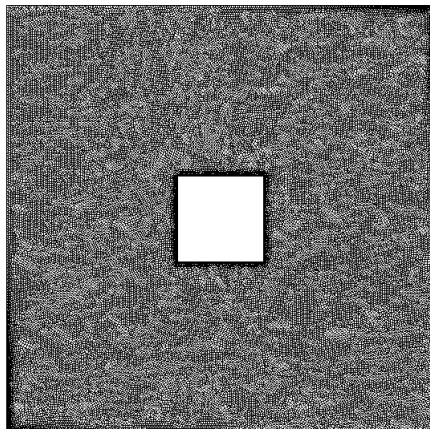
where Res is the “largest variable residual” in the whole computational domain in two successive time steps and Var is the variable (velocity or temperature) magnitude in each point in the grid.

Both variables have to reach the convergence criterion in order to drop computing. The velocity field lasts more than the temperature field to achieve convergence.

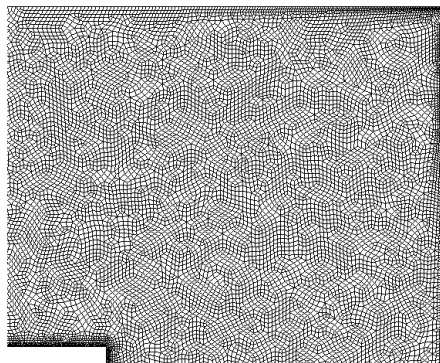
4. Results and discussion

Figure 4 depicts the isotherms and streamlines for Grashof numbers 10^3 , 10^4 , and 10^5 , and $Re = 50$, 100 , and 500 . The nanoparticle volume fraction ϕ (PHI) is 1% due to physical correlations applied in this work. Overall, there is flow recirculation caused by geometry and boundary conditions. They appear near the zone where the nanofluid enters the cavity, in the lower right edge, and near the heat source. Recirculation presence can be explained by the fact that the flow faces a zone with relevant pressure and that it deviates from its original way to a different one. Those higher pressure zones may occur when one flow impairs the way of the other flow. This effect can be plainly noted in the situations where forced velocities, present in the main flow, are more significant. For instance, for Reynolds number equal to 100 , the nanofluid flow, which goes upwards because of buoyancy forces and the adjacent main flow, does not possess energy sufficient to pass through the main flow in order to exit the cavity. This behavior creates minor flows that are jailed near the heated module. For that being so, it creates a region which has higher temperatures. As indicated Figure 4, in the cases which go from left to right and from top to bottom, the zone which is highly heated is located in the upper left corner of

the heat source. This behavior regards to in what degree the main flow, which begins from the entrance region and goes in the direction of the exit opening and flows below the heat source, becomes more significant. The more powerful the main flow is, the tougher is it for the flow to break through that main velocity wake. If a producer of heat exchangers has the opportunity to modify an equipment design, the case which brings forced velocities downstairs and opposite to the upward buoyancy forces, may provide a little increase in heat transfer. Finally, in order to estimate any conclusion, it is necessary the performance in more studies. If Grashof number is kept $Gr = 10^4$ and 10^5 , the temperature on the heated module increases when strengthening the forced velocity where nanofluid goes in. In general, one should expect the heat transfer to enhance when increasing Reynolds number. Nevertheless, one may observe that it may be different. For $Gr = 10^4$, the highest temperature varies from 0.240 to 0.3187 as Reynolds number goes from 50 to 500. Moreover, the highest temperature varies from 0.2539 to 0.3045 for the same Re limits and $Gr = 10^5$. Hence, not only the geometry, but also boundary conditions, may bring inconsistency to what readers are used to facing. These contradictions are explained by the presence of those recirculations mentioned previously which are stuck in a certain zone of the domain.



a) Entire domain



b) Partial domain (right upper corner)

Figure 3. Unstructured mesh with linear quadrilateral elements.

Figure 5 illustrates the comparison between the Nusselt number and the Reynolds number for Gr equal to 10^3 , 10^4 , 10^5 and $\phi = 0$ and 1% . Overall, the Nusselt number does not enhance with Re for the reason that was mentioned before. However, the Nusselt number enhancement is of lower level. The nanoparticle volume fraction seems to increase heat transfer for $\phi = 1\%$, though. This cannot be the case for situation 15 where one expects the high thermal conductivity of copper to enhance heat transfer. One should see in case 15 that gradients in temperature are weaker on the upper left zone. It is noteworthy to mention that more studies are necessary to be performed in order to analyze such case when $Gr = 10^4$ and $Re = 500$.

Table 4 shows some Nusselt number values and the maximum value of temperature on the heated module for the two nanoparticle volume fractions ($\phi = 0$ and 1%). In an overall view, the enhancement of heat transfers on the heated module, where cooling is expected, is of the order of 0.04. Such level is not high. It may appear very meaningful when it comes to terms of heat exchanger performance and manufacturing, though.

Figure 6 indicates isotherms and streamlines for $Gr = 10^3$ to 10^5 , and $Re = 50$ to 500 , volume fraction equal to 0.1 for forced convection in the descending direction. One may observe similar behaviors when considering the ascending forced convection. Here, stuck flow around the square heat source are also present. However, almost every case shown in Figure 5 undergoes such behavior. The primary flow passes over the heated source for the cases where Re are high (500) and the forced convection is more significant. In a general manner, one should avoid using cases where the flow is jammed around the heat sources. In cases 45, 46 and 47, the primary flow changes its position when taking the heat source as reference. In cases 45 and 46, buoyancy forces are strong enough to bring about a high pressure region that forces the primary flow below the heat source. On the other hand, for $Re = 500$, the flow is sufficiently powerful to break through that area and forces its way into the region just above the heat source.

Figure 7 illustrates the mean Nusselt number on the heated module against Reynolds number range for $Gr = 10^3$ to 10^5 and concentrations 0 and 1% . There is a quite intriguing result here. For $Gr = 10^3$ and 10^4 , Nusselt number behaves quite similar to the correlated problems in the ascending forced convection. However, its behavior for $Gr = 10^5$ is quite contrary to its corresponding case in the ascending forced convection. That is, the Nusselt number has a tendency to increase when strengthening forced flows. This is caused by the position change of the primary forced flow and the position change of the jammed recirculation regions nearby the heat source. These recirculation directions are similar. Both directions are counterclockwise.

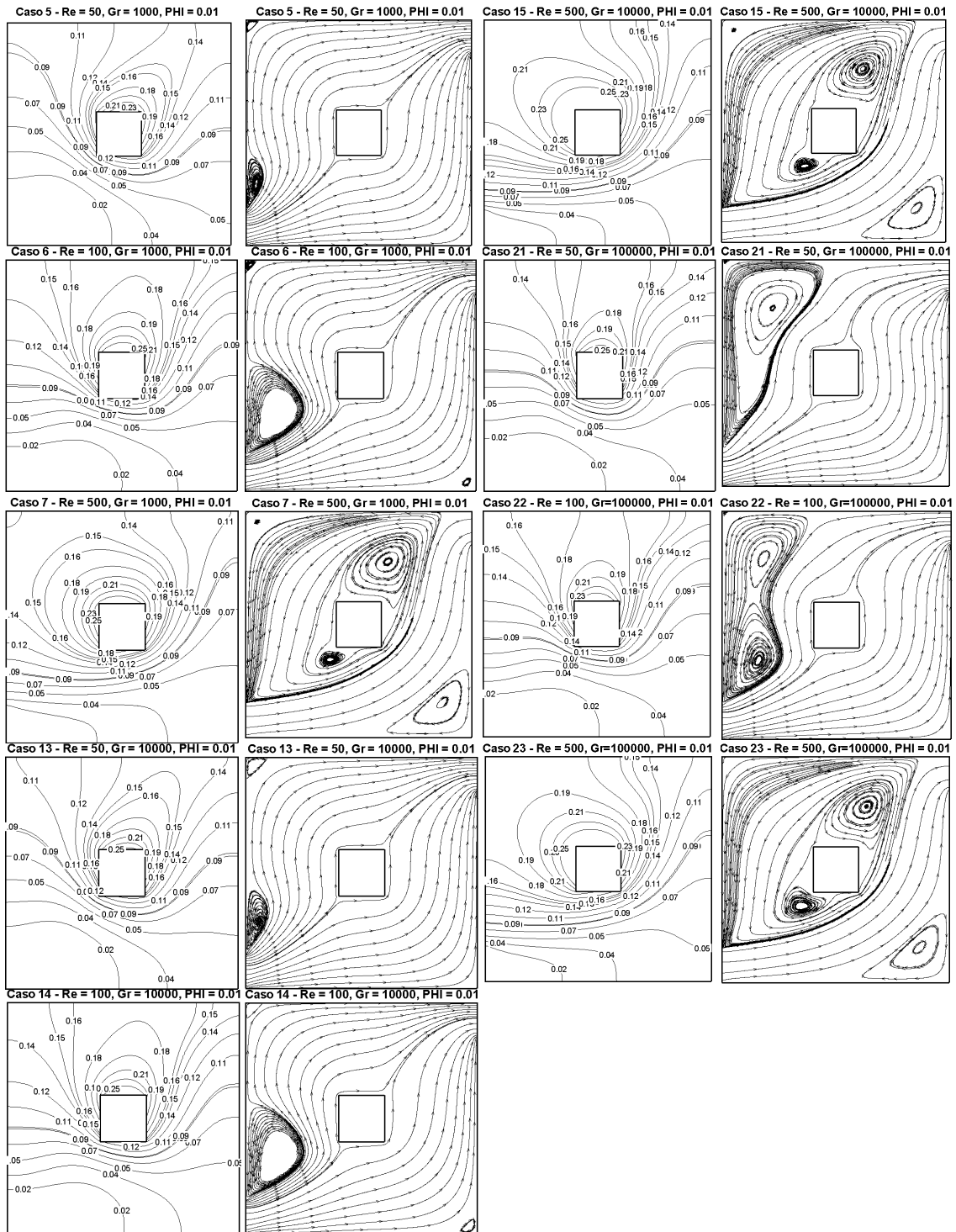


Figure 4. Isotherms and streamlines for cases with Gr = 103, 104, and 105, and Re = 50, 100, 500, PHI = 0.1.

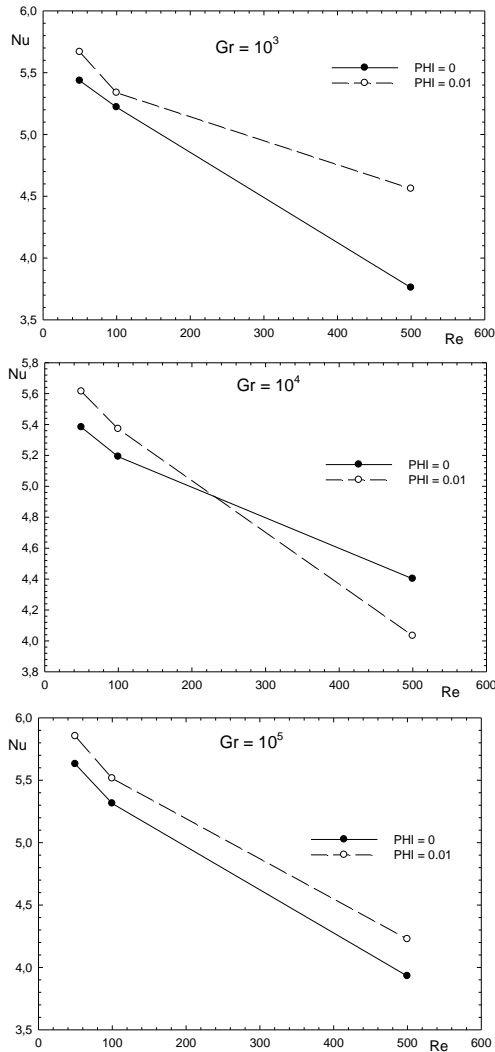


Figure 5. Nu for Gr = 103, 104, 105, PHI = 0 and 1%.

5. Conclusion

A mixed convection study was performed in a square ventilated cavity with an inner heated module. The working fluid was a Copper/water nanofluid. Two volume fractions were used (0 and 1%). Reynolds numbers ranged from 5×10^1 to 5×10^2 and the Grashof number from 10^3 to 10^5 . The direction of the entrance flow towards the exit flow was not only in favor of, but also contrary to the buoyancy forces, that is, upward and downward paths of the main flow, respectively. When applying forced flows in the ascending way, this present study brought about an interesting effect as the Reynolds number increased with constant Grashof number. It might have been expected from such behavior that heat transfer should increase with Reynolds number being increased. Nonetheless, quite the contrary occurred. This is due to a set of parallel effects: the geometrical features and the forced velocities. With the growth of Re, the energy and size of the recirculation near the heated module were more significant. Consequently, this made it become more difficult to the lower temperature nanofluid to reach the heated module. The fluid was jailed nearby the heated module since it did not possess enough energy to pass the path with relevant pressure. In a general

manner, when one concerned ascending cases, the nanoparticle volume fraction effect on Nusselt number augmentation was the order of 0.04 (4%) for cases, with volume fractions equal to 0 (pure water) and 1%. The authors reinforce that, for high Reynolds numbers, mass and energy conservation should be more investigated when applying the parameters applied in the present work. When the primary flow was descending, the Nusselt number increased when increasing forced flows.

Table 4. Values of Tmax on the heat source and Nusselt number for $\phi = 0$ and 1%.

Case	Re	Gr	Nusselt	TMAX
			$\phi = 0$	
1	50	103	5.4342	0.255
2	100	103	5.2194	0.2849
9	50	104	5.3822	0.2639
10	100	104	5.1920	0.2973
17	50	105	5.6288	0.2632
18	100	105	5.3130	0.2846
Case	Re	Gr	$\phi = 0.01$	
			5.6665(4%)	0.246(-4%)
6	100	103	5.3369(2%)	0.2811(-1%)
13	50	104	5.6133(4%)	0.254(-4%)
14	100	104	5.3711(3%)	0.2796(-6%)
21	50	105	5.8528(4%)	0.2539(-4%)
22	100	105	5.5139(4%)	0.2757(-3%)

Acknowledgements

The authors thank Fapemig for the financial support from the Process APQ-02457-12.

Nomenclature

- Gr Grashof number
- H Cavity height
- h Heat transfer coefficient
- k_{nf} Nanofluid thermal conductivity
- Nu_{hs}^* Nusselt number on the heat source
- P Dimensionless pressure
- p Dimensional pressure
- Pr Prandtl number
- q'' Dimensionless heat flux
- Ra Rayleigh number
- Re Reynolds number
- Ri Richardson number
- S Surface
- T Dimensional temperature
- t Dimensional time
- U, V Dimensionless velocities
- u, v Dimensional velocities
- x, y Dimensional coordinates
- X, Y Dimensionless coordinates

Greek symbols

- α_{nf} Nanofluid thermal diffusivity

Δ Increment
 θ Dimensionless temperature
 μ_{nf} Nanofluid dynamic viscosity
 ν Kinematics viscosity
 ρ_{nf} Nanofluid density
 $(\rho\beta)_{nf}$ Nanofluid thermal expansion
 $(\rho C_p)_{nf}$ Nanofluid heat capacitance
 ϕ Nanoparticle concentration

τ Dimensionless time
Subscripts
 c, h Cold and hot surfaces
 hs heat source
 f Pure fluid
 nf Nanofluid
 p Particle

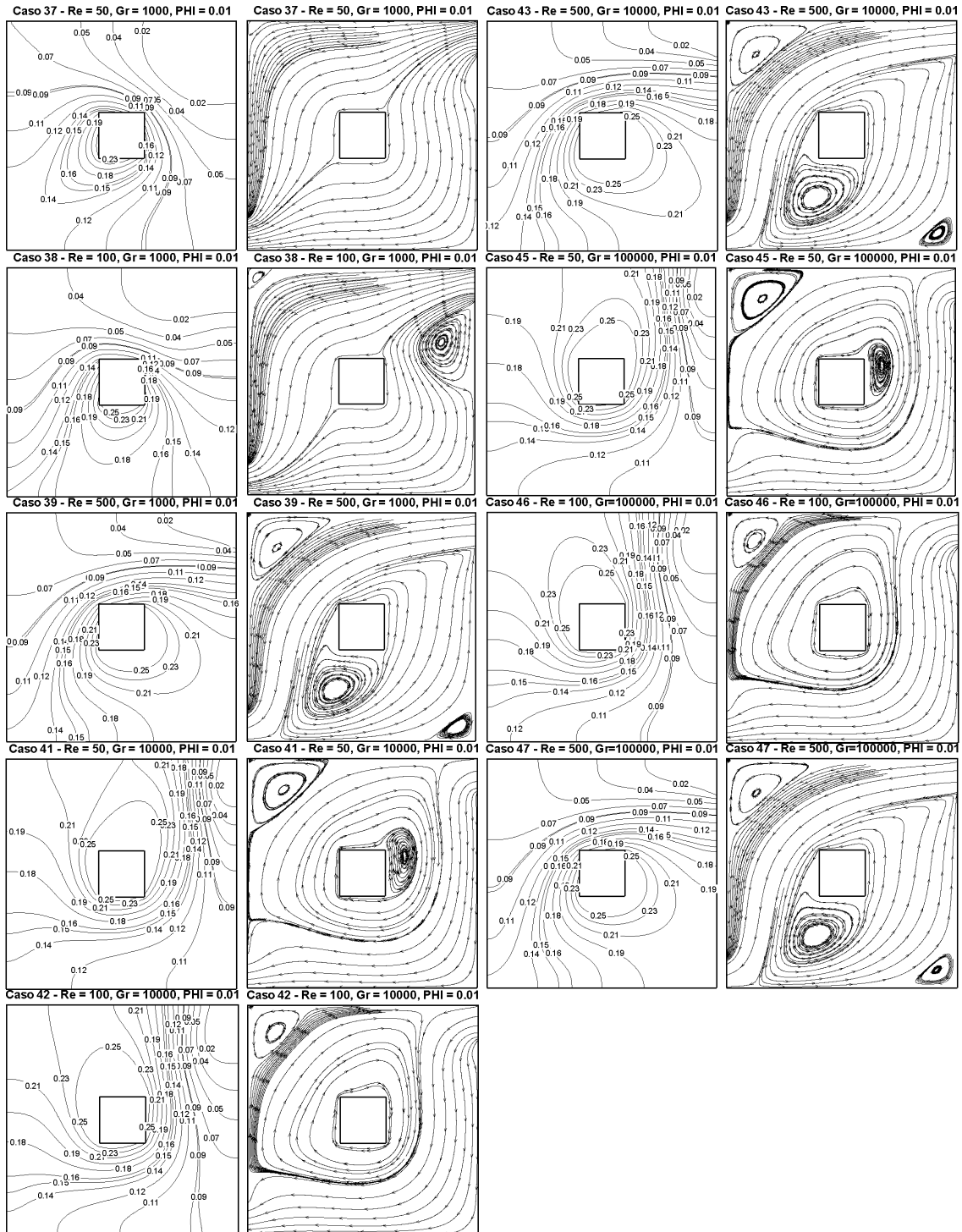


Figure 6. Isotherms and streamlines for cases with Gr = 103, 104, and 105, and Re = 50, 100, 500, PHI = 0.1.

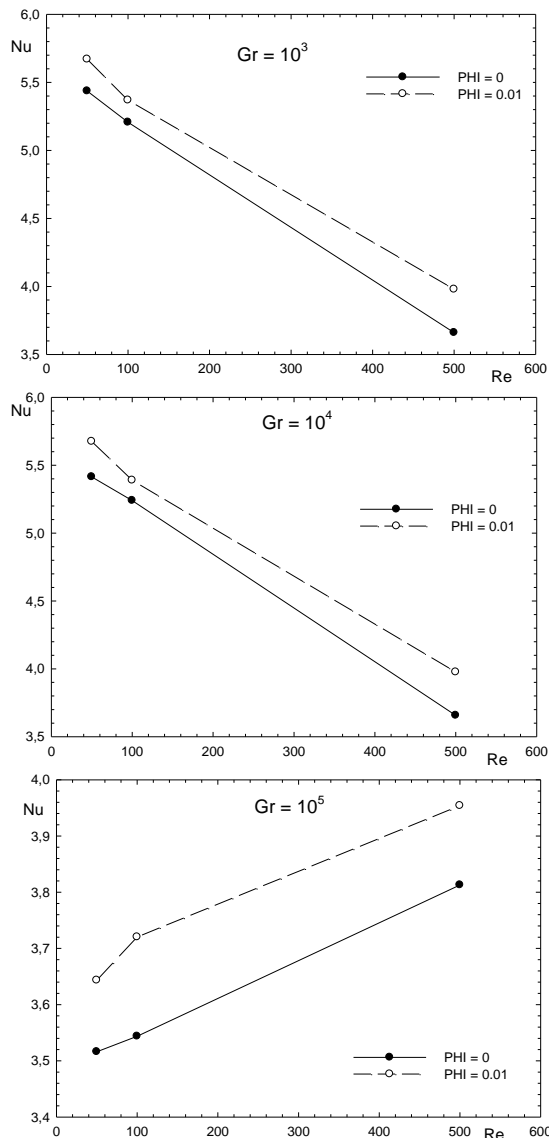


Figure 7. Nusselt versus Reynolds number for $Gr = 10^3$, 10^4 and 10^5 for $\text{PHI} = 0$ and 1%.

References

[1] H. Moumni, H. Welhezi, E. Sediki, Numerical Investigation of Heat Transfer Enhancement in a Square Ventilated Cavity with Discrete Heat Sources Using Nanofluid, *Heat and Mass Transfer and Physical Gasdynamics*, 55 (3), 426-433, (2017).

[2] F. F. Hinojosa, N. A. Rodriguez, J. Xamán, Heat transfer and airflow study of turbulent mixed convection in a ventilated cavity, *Journal of Building Physics*, 204-234, (2015).

[3] E. Arquís, M. A. Rady, A. S. Nada, A numerical investigation and parametric study of cooling an array of multiple protruding heat sources by a laminar slot air jet, *International Journal of Heat and Fluid Flow*, 28, 787-800, (2007).

[4] G. M. Rao and G. S. V. L. Narasimham, Laminar conjugate mixed convection in a vertical

channel with heat generating components, *International Journal of Heat and Mass Transfer*, 50, 3561-3574, (2007).

- [5] M. Shahi, A. H. Mahmoudi, F. Talebi, Numerical study of mixed convective cooling in a square cavity ventilated and partially heated from the below utilizing nanofluid, *International Communications in Heat and Mass Transfer*, 37, 201-213, (2010).
- [6] T. H. Nassan, S. Z. Heris, S. H. Noie, A comparison of experimental heat transfer characteristics for Al₂O₃/water and CuO/water nanofluids in square cross-section duct, *International Communications of Heat and Mass Transfer*, 37, 924-928, (2010).
- [7] M. Rostamani, S. F. Hosseinizadeh, M. Gorji, J. M. Khodadadi, Numerical study of turbulent forced convection flow of nanofluids in a long horizontal duct considering variable properties, *International Communications in Heat and Mass Transfer*, 37(10), 1426-1431, (2010).
- [8] R. Lotfi, Y. Saboohi, and A.M. Rashidi, Numerical study of forced convective heat transfer of Nanofluids: Comparison of different approaches, *International Communications in Heat and Mass Transfer*, 37, 74-78, (2010).
- [9] J. Jung, H. Oh, H. Kwak, Forced convective heat transfer of nanofluids in microchannels, *International Journal of Heat and Mass Transfer* 52, 466-472, (2009).
- [10] A. Arefmanesh and M. Mostafa, Effects of uncertainties of viscosity models for Al₂O₃-water nanofluid on mixed convection numerical simulations, *International Journal of Thermal Sciences*, 50, 1706-1719, (2011).
- [11] T. Behzardi, K. M. Shirvan, S. Mirzakhani, A. A. Sheikhrobat, *Procedia Engineering*, 127, 221-228, (2015).
- [12] H. C. Brinkman, The viscosity of concentrated suspensions and solution, *Journal of Chemical Physics*, 20, 571-581, (1952).
- [13] J. Maxwell, *A treatise on electricity and magnetism*, second ed., Oxford University Press, Cambridge, UK (1904).
- [14] S. M. Aminossadati, B. Ghasemi, Natural convection cooling of a localized heat source at the bottom of a nanofluid-filled enclosure, *European Journal of Mechanics B/Fluids*, 28, 630-640, (2009).
- [15] C. J. Ho, M. W. Chen, Z. W. Li, Numerical simulation of natural convection of nanofluid in a square enclosure: effects due to uncertainties of viscosity and thermal conductivity, *International Journal of Heat and Mass Transfer*, 51(17-18), 4506-4516 (2008).

- [16]H. F. Oztop, E. Abu-Nada, Numerical study of natural convection in partially heated rectangular enclosures filled with nanofluids, *International Journal of Heat and Fluid Flow*, 29(5), 1326-1336, (2008).
- [17]R. J. Krane, J. Jessee, Some detailed field measurements for a natural convection flow in a vertical square enclosure, *Proceedings of the First ASME-JSME Thermal Engineering Joint Conference*, 1, 323-329, (1983).
- [18]K. Khanafer, K. Vafai, M. Lightstone, Buoyancy-driven heat transfer enhancement in a two-dimensional enclosure utilizing nanofluids, *International Journal of Heat and Mass Transfer*, 46, 3639-3653, (2003).
- [19]FIDAP Theoretical Manual, Fluid Dynamics International, Evanston, IL, USA (1990).
- [20]G. Barakos, E. Mitsoulis, Natural convection flow in a square cavity revisited: laminar and turbulent models with wall functions, *International Journal of Numerical Methods in Fluids*, 18, 695-719, (1994).
- [21]De Val Davis, Natural convection of air in a square cavity, a benchmark numerical solution, *International Journal of Numerical Methods in Fluids*, 3, 249-264, (1962).
- [22]T. Fusegi, J. M. Hyun, K. Kuwahara, B. Farouk, A numerical study of three-dimensional natural convection in a differentially heated cubical enclosure, *International Journal of Heat and Mass Transfer*, 34, 1543-1557, (1991).